Published in final edited form as:
Neurobiol Dis. 2009 May ; 34(2): 308–319. doi:10.1016/j.nbd.2009.02.001.

Progressive thalamocortical neuron loss in *Cln5* deficient mice: distinct effects in Finnish variant late infantile NCL

Carina von Schantz[1], **Catherine Kielar**[2,*], **Stine N Hansen**[2,*], **Charlie C Pontikis**[2], **Noreen A Alexander**[2], **Outi Kopra**[3], **Anu Jalanko**[1], and **Jonathan D Cooper**[2]

[1]National Public Health Institute, Department of Molecular Medicine and FIMM, Institute for Molecular Medicine Finland, Biomedicum Helsinki, Finland [2]Pediatric Storage Disorders Laboratory, Department of Neuroscience and Centre for the Cellular Basis of Behaviour, MRC Centre for Neurodegeneration Research, Institute of Psychiatry, King's College London, UK [3]Department of Medical Genetics, Folkhälsan Institute of Genetics and Neuroscience Center, University of Helsinki, Finland

Abstract

Finnish variant LINCL (vLINCL$_{Fin}$) is the result of mutations in the *CLN5* gene. To gain insights into the pathological staging of this fatal pediatric disorder, we have undertaken a stereological analysis of the CNS of *Cln5* deficient mice (*Cln5*$^{-/-}$) at different stages of disease progression. Consistent with human vLINCL$_{Fin}$, these *Cln5*$^{-/-}$ mice displayed a relatively late onset regional atrophy and generalized cortical thinning and synaptic pathology, preceded by early and localized glial responses within the thalamocortical system. However, in marked contrast to other forms of NCL, neuron loss in *Cln5*$^{-/-}$ mice began in the cortex and only subsequently occurred within thalamic relay nuclei. Nevertheless, as in other NCL mouse models, this progressive thalamocortical neuron loss was still most pronounced within the visual system. These data provide unexpected evidence for a distinctive sequence of neuron loss in the thalamocortical system of *Cln5*$^{-/-}$ mice, diametrically opposed to that seen in other forms of NCL.

Keywords

Finnish variant late infantile neuronal ceroid lipofuscinosis; Batten disease; CLN5; Thalamocortical neurodegeneration; Lysosomal storage disorder

Introduction

The Neuronal Ceroid Lipofuscinoses (NCLs) are collectively the most common group of inherited pediatric neurodegenerative diseases. Their clinical symptoms include visual impairment, seizures, progressive psychomotor retardation and premature death (Santavuori, 1988). The NCLs are pathologically defined by a dramatic loss of CNS neurons, but with very few obvious effects outside the brain. All forms of NCL exhibit the characteristic accumulation

Address for correspondence: Jonathan D. Cooper, Pediatric Storage Disorders Laboratory, Department of Neuroscience and Centre for the Cellular Basis of Behaviour, James Black Centre, Institute of Psychiatry, King's College London, 125 Coldharbour Lane, London, SE5 9NU, UK. Phone +44-20-7848-0286; Fax +44-20-7848-0986; E-mail: E-mail: j.cooper@iop.kcl.ac.uk.
*These authors contributed equally to this study

of lysosomal autofluorescent lipopigments that display subtype specific ultrastructure (Mole et al., 2005). The NCLs are classified into ten different subtypes (CLN1-CLN10) on the basis of age of onset, clinicopathological features and genetic linkage, with eight genes identified to date (Siintola et al., 2006, 2007).

The Finnish variant form of Late Infantile Neuronal Ceroid Lipofuscinosis (vLINCL$_{Fin,}$ CLN5) is caused by mutations in the *CLN5* gene, originally reported as encoding both soluble and membrane-bound forms of a lysosomal protein (Isosomppi, et al., 2002; Vesa et al., 2002). vLINCL$_{Fin}$ typically appears between 4-7 years of age, with the first symptoms usually being motor clumsiness followed by progressive visual failure and blindness, motor and mental deterioration, myoclonia and seizures culminating in an early death between 14 and 36 years (Santavuori, 1993; Santavuori, 1982). Although the function of the CLN5 protein has remained elusive, the consensus view is that its predominant form is a soluble lysosomal protein (Sleat et al., 2005).

Several animal models exist for different forms of NCLs and they provide excellent tools for thorough characterization of temporal and spatial pathological cascades (Cooper, 2003; Cooper et al., 2006). Mouse models of NCL share several common pathological similarities, including selective loss of GABAergic interneuron subpopulations, cortical and thalamic atrophy and pronounced early gliosis (reviewed in Mitchison et al., 2004; Cooper et al., 2006). More detailed pathological analyses of mouse models of congenital, infantile and juvenile forms of NCL, have all highlighted the thalamocortical pathways in pathogenesis with an early loss of thalamic relay neurons before the onset of neuron loss within the corresponding cortical region (Pontikis et al., 2005; Weimer et al., 2006; Kielar et al., 2007; Partanen et al., 2008).

Consistent with the milder NCL-phenotype of human vLINCL$_{Fin}$ patients, *Cln5*$^{-/-}$ mice exhibit rather mild clinical symptoms (Kopra et al., 2004). These mice show widespread CNS accumulation of autofluorescent material, progressive visual failure and effects upon GABAergic interneuron survival (Kopra et al., 2004). Gene expression profiling of *Cln5*$^{-/-}$ mice revealed changes in the CNS expression levels for genes related to phosphorylation, cell adhesion, inflammation and myelin integrity (Kopra et al., 2004; von Schantz et al. 2008). Nevertheless, no detailed information is available about the sequence of neuropathological changes in these *Cln5*$^{-/-}$ mice. Since the thalamocortical system displays a series of localized neurodegenerative and reactive changes in other models of NCL (Pontikis et al., 2005; Weimer et al., 2006; Kielar et al., 2007; Partanen et al., 2008), we focused our analysis on these pathways. Although *Cln5* deficient mice share many similar features with other mouse models of NCL, our findings reveal that the sequence of neuron loss is unexpectedly different in *Cln5*$^{-/-}$ mice, starting in the cortex and only subsequently becoming apparent in the thalamus.

Materials and methods

Animals

Homozygous mutant *Cln5*$^{-/-}$ mice were generated on a mixed C57BL/6Jx129SvEv strain background as described previously (Kopra et al., 2004; Jalanko et al., 2005) and subsequently backcrossed for three generations with C57Bl/6 controls to produce the mice used in this study. To provide a direct comparison with another NCL mouse model raised on the same strain background and housed in the same animal facility, we also collected brain tissue from male *Cln1*$^{-/-}$ (*Ppt1*$^{\Delta ex4}$) mice (Jalanko et al., 2005) at 1 and 4 months of age. We utilized systematically sampled brain tissue from 1, 4 and 12 month old male mice for all experiments with separate wild-type littermate mice used as controls for each mutant strain. The genotypes of all mice were determined by polymerase chain reaction of DNA from tail biopsies (Kopra et al., 2004; Jalanko et al., 2005). All animal experiments were conducted in accordance with

international standards on animal welfare and with approved animal policies of the National Public Health Institute, Helsinki, with adequate measures taken to minimize pain or discomfort.

Histological processing

For histological analysis, *Cln5*$^{-/-}$, *Cln1*$^{-/-}$ and age-matched control mice (n = 3 per genotype and age) were euthanized at 1 month and 4 months of age (both strains of mutant mice) and 12 months of age (*Cln5*$^{-/-}$ only) in a rising concentration of carbon dioxide, their brains removed and bisected along the midline. One half of the bisected brain was frozen in liquid nitrogen and stored in -70°C and the other hemisphere was fixed in 4% paraformaldehyde in 0.2M phosphate buffer for at least one week before cryoprotection in 30% sucrose in 50mM Tris buffered saline (TBS) containing 0.05% Sodium Azide. From these cryoprotected brains 40 μm frozen coronal sections were cut through the cortical mantle (Leitz 1321 freezing microtome, Leica Microsystems, Welwyn Garden City, UK), while the cerebellum was cut sagittally. As described previously sections were collected, one per well, into 96 well plates containing a cryoprotectant solution (Bible et al., 2004; Kielar et al., 2007), and stored at −80° C before histological processing. To provide direct visualization of neuronal morphology each adjacent section was slide mounted and Nissl stained as described previously (Bible et al., 2004). All histological processing and subsequent analyses were performed with no prior knowledge of genotype or treatment group.

Regional volume measurements

To examine regional volume, unbiased Cavalieri estimates of the cortex, hippocampus, striatum, thalamus, hypothalamus and cerebellum were performed from 40 μm Nissl-stained cryosections, as described previously (Bible et al., 2004; Pontikis et al., 2004). A sampling grid with appropriate spacing was superimposed over each section, and the number of points covering the relevant areas counted using objectives of appropriate magnification and *StereoInvestigator* software (Microbrightfield Inc., Williston, VT). Regional volumes were expressed in μm^3 and the mean volume of each region calculated for the *Cln5*$^{-/-}$ mice and controls.

Cortical thickness measurements

To explore the extent of cortical atrophy cortical thickness measurements were made on the same one-in-six series of Nissl stained sections for primary motor (M1), primary somatosensory (S1BF), primary visual (V1) and lateral entorhinal (LEnt) cortex using an x1.25 objective as described previously (Bible et al., 2004; Pontikis et al., 2004), using anatomical landmarks defined in Paxinos and Franklin (2001). On each of three consecutive sections, the length of perpendicular lines extending from the white matter to the pial surface was measured by placing ten evenly spaced lines spanning each cortical region. Results were expressed as mean cortical thickness in μm per region for *Cln5*$^{-/-}$ mice and controls. Individual laminar thickness were also measured in M1, S1BF, V1 and LEnt using the same three consecutive Nissl-stained sections. The thickness of each individual lamina was measured via ten perpendicular lines using an x10 objective. Results were expressed as mean laminar thickness in μm per region for *Cln5*$^{-/-}$ mice and controls.

Counts of neuronal number

To examine neuronal survival and volume within individual thalamic nuclei and their target cortical regions we used *StereoInvestigator* software to obtain unbiased optical fractionator estimates of the number of Nissl stained neurons in each structure, with the boundaries of each nucleus as defined by Paxinos and Franklin (2001). These measures were performed in the ventral posterior nucleus (VPM/VPL), dorsal lateral geniculate nucleus (LGNd), which project to S1BF and V1, respectively. In these cortical regions we obtained optical fractionator

estimates of the number of Nissl stained granule neurons in lamina IV granule neurons that receive thalamic innervation, lamina VI neurons that supply feedback to the thalamus, and lamina V projection neurons. These measures were performed exactly as described previously (Bible et al., 2004; Kielar et al., 2007), with a random starting section chosen, followed by every sixth Nissl stained section. All counts carried out using an x100 oil objective (NA 1.4), with only neurons with a clearly identifiable nucleolus counted.

Immunohistochemistry

To asses the extent of glial activation, adjacent one-in-sixth series of free floating 40 μm frozen sections were immunohistochemically stained, as described previously (Bible et al., 2004), for detection of astrocytic (GFAP, DAKO, Cambridge, UK, 1:5000) and microglial (F4/80, Serotec, Oxford, UK, 1:100) markers. Briefly, sections were incubated for 15 min in 1% hydrogen peroxide in TBS to quench endogenous peroxidase activity, rinsed in TBS and incubated for 40 min in TBS/0.3% Triton X-100 (TBS-T) containing 15% normal serum to block non-specific binding of immunoglobulins. Sections were incubated overnight at 4°C in primary antiserum diluted with 10% normal serum in TBS-T, and subsequently rinsed in TBS and incubated for two hours in biotinylated secondary antiserum diluted with 10% normal serum in TBS-T. Following rinsing in TBS, sections were incubated for two hours in Vectastain avidin-biotin-peroxidase complex (Elite ABC kit, Vector Laboratories, Peterborough, UK) diluted with 10% normal serum in TBS-T and rinsed again in TBS. Immunoreactivity was visualized by a standard DAB reaction (Sigma, Dorset, UK), and sections transferred to excess ice-cold TBS, onto gelatine-chrome alum coated Superfrost microscope slides (VWR, Dorset, UK), air-dried overnight and passed through a graded series of alcohol before clearing in xylene and coverslipping with DPX mounting media (VWR).

Quantitative analysis of glial phenotype

The optical density of GFAP and F4/80 immunoreactivity was assessed using a semi-automated thresholding image analysis, as previously described (von Eitzen et al., 1998; Bible et al., 2004; Kielar et al., 2007), with each marker analyzed blind with respect to genotype or age. Briefly, 40 nonoverlapping images, on triplicate sections, were captured through each selected brain region (GFAP and F4/80: VPM/VPL and S1BF). The optimal segmentation of immunoreactive profiles was determined using *Optimas* image analysis software (Media Cybernetics, Silver Springs, MD) using a previously described semi-automated thresholding method based on the optical density of the reaction product (von Eitzen et al., 1998; Bible et al., 2004; Kielar et al., 2007). Macros were recorded to transfer the data to a spreadsheet for subsequent statistical analysis. Data were plotted graphically as the mean percentage area of immunoreactivity per field ± SEM for each region.

Statistical analysis

The statistical significance of differences between genotypes of all quantitative data was assessed using a one-way ANOVA (SPSS 11.5 software, SPSS Inc, Chicago, IL), with statistical significance considered at $P \leq 0.05$. The mean co-efficient of error (CE) for all individual optical fractionator and Cavalieri estimates was calculated according to the method of Gundersen and Jensen (1987) and was less than 0.08 in all these analyses.

Results

Regional atrophy and cortical thinning in *Cln5*$^{-/-}$ mice

Apart from an early and progressive visual failure *Cln5* null mutant mice (*Cln5*$^{-/-}$) display a relatively late onset disease phenotype (Kopra et al., 2004). To survey effects upon the CNS in symptomatic mutant mice, we carried out a stereological survey of regional volume in Nissl-

stained sections of *Cln5*$^{-/-}$ mice and littermate controls at 12 months of age. Cavalieri estimates of regional volume revealed significant atrophy of the cortex, hippocampus, striatum and thalamus of these aged *Cln5*$^{-/-}$ mice, but no significant effects upon the volume of the hypothalamus and cerebellum (Figure 1A).

Cortical atrophy is a consistent feature of all forms of human and murine NCL (Cooper et al., 2006), but does not usually occur equally across the cortical mantle (e.g. Bible et al., 2004; Kielar et al., 2007). To investigate whether similar regional effects were apparent in *Cln5* deficient mice, we made thickness measurements in Nissl stained sections through the primary motor cortex (M1), somatosensory barrelfield cortex (S1BF), primary visual cortex (V1), and lateral entorhinal cortex (LEnt), as representative cortical regions that serve different functions. Compared with littermate controls, 12 month old *Cln5*$^{-/-}$ mice exhibited significant thinning in all cortical regions (Figure 1B), suggesting widespread rather than regionally specific effects upon the cortical mantle.

To determine whether the reduced thickness of these cortical regions was due to laminar specific events, we made a series of individual laminar thickness measurements in the same Nissl stained sections (Figures 2A-D). These measurements revealed more pronounced effects upon deeper cortical laminae in *Cln5* deficient mice, with significant thinning of lamina V in all four cortical regions (Figures 2A-D), and significant thinning of laminae IV and VI in S1BF, V1 and LEnt (Figures 2B-D). In contrast, more superficial laminae exhibited a series of complex series of changes in thickness in 12 month old *Cln5*$^{-/-}$ mice. For example, M1, S1BF and V1 of *Cln5* mutant mice displayed a significantly increased thickness of laminae I and II/III (Figures 2B-D), and a significant reduction in thickness of lamina I, and a significantly increased thickness of lamina III within LEnt (Figure 2D).

Synaptic pathology in *Cln5* deficient mice

Mouse models of congenital, infantile and juvenile NCL display a range of synaptic pathologies (Partanen et al., 2008; Kim et al., 2008; Kielar, Gillingwater and Cooper, unpublished observations), which are most pronounced within the somatosensory and visual thalamocortical pathways. To determine whether severely affected *Cln5*$^{-/-}$ mice display a similar phenotype, we stained sections from these mice for a range of pre-synaptic markers, including the synaptic vesicle protein synaptobrevin, the pre-synaptic membrane protein synaptophysin and the SNARE complex protein SNAP25. We concentrated our analysis upon the ventral posterior thalamic nucleus (VPM/VPL) and the dorsal lateral geniculate nucleus (LGNd), which relay sensory information to the primary somatosensory (S1BF) and primary visual (V1) cortical subfields, respectively and display pronounced synaptic pathology in Cathepsin D deficient mice (Partanen et al., 2008). Immunohistochemical staining for these proteins revealed pronounced changes in the intensity and distribution of staining for these markers in the thalamocortical system of 12 month old *Cln5*$^{-/-}$ mice. In these severely affected mutant mice, SNAP25 and synaptophysin immunoreactivity were markedly reduced in both VPM/VPL and LGNd of 12 month old *Cln5*$^{-/-}$ mice, where as VAMP2 immunoreactivity appeared upregulated and around the persisting neurons in these thalamic nuclei (Figure 3A, 3B). Changes in staining for synaptic markers were also evident in the corresponding cortical regions of these severely affected mutant mice, with markedly decreased staining for synaptophysin and redistribution of VAMP2 immunoreactivity in both S1BF and V1. However, in marked contrast to the thalamus, SNAP25 immunoreactivity was relatively preserved in the cortex of 12 month old *Cln5*$^{-/-}$ mice and displayed similar staining intensity in S1BF and V1 of mice of both genotypes (Figure 3C). Taken together these data provide the first evidence for synaptic pathology in *vLINCL*$_{Fin}$, and suggest that this may be different in nature in the thalamus and cortex of *Cln5* deficient mice.

Localized reactive changes in the thalamocortical system of *Cln5*$^{-/-}$ mice

Mouse models of NCL consistently display localized and progressive glial activation, which typically precedes neuron loss and is associated with synaptic pathology (Cooper et al., 2006; Partanen et al., 2008), with the thalamocortical system emerging as a particular focus for these events (e.g. Bible et al., 2004, Pontikis et al., 2005, Kielar et al., 2007; Partanen et al., 2008). To determine whether *Cln5* deficient mice share this phenotype, we examined adjacent series of sections from control and mutant mice between 1 and 12 months of age stained with the astrocytic marker GFAP (Figure 4) or the microglial marker F4/80 (Figure 6). As representative nuclei that display pronounced reactive changes in mouse models of congenital, infantile and juvenile NCL (Pontikis et al., 2005; Weimer et al., 2006; Kielar et al., 2007; Partanen et al., 2008), we again concentrated our analysis upon the thalamic nuclei VPM/VPL, and LGNd, together with S1BF and V1, the cortical regions to which these nuclei relay sensory information.

Astrocytosis—In both S1BF and V1 of control mice of all ages only few GFAP-immunoreactive astrocytes were present (Figures 4A and 4C), predominantly in laminae I and VI, with additional scattered positive cells in lamina V. At 1 month of age the distribution of GFAP immunoreactivity in S1BF (Figure 4A) and V1 (Figure 4C) was similar in *Cln5*$^{-/-}$ mice. However, in these mutant mice at 4 months of age the number and density of GFAP stained protoplasmic astrocytes was increased within all laminae of S1BF (Figure 4A) and V1 (Figure 4C), with the exception of lamina IV, which contained very few positively stained astrocytes in either cortical region. At 12 months of age both cortical regions exhibited widespread astrocytosis in *Cln5* deficient mice, with intensely GFAP-immunoreactive astrocytes present in all laminae (Figure 4A and 4C).

In the thalamus, *Cln5*$^{-/-}$ mice displayed a progressive astrocytosis that became more pronounced with increased age (Figure 4B and 4D). Within VPM/VPL, numerous scattered GFAP-positive astrocytes were already evident in mutant mice at 4 months of age (Figure 4B), but were virtually absent in age-matched controls. By 12 months of age intense GFAP immunoreactivity was now evident throughout VPM/VPL, spreading into adjacent nuclei (Figure 4B). In contrast, there was no discernable difference in the distribution of GFAP immunoreactivity in LGNd (Figure 4D) or MGN (data not shown) of mutant and control mice, until 12 months of age when both of these nuclei were completely filled with intensely immunoreactive astrocytes in *Cln5* deficient mice.

Quantitative thresholding image analysis confirmed the significantly increased astrocytosis within both VPM/VPL (Figure 5A) and S1BF (Figure 5B) of *Cln5* deficient mice with increased age. Consistent with our histological observations this increased astrocytosis was of greater magnitude in the thalamus of mutant mice at each age examined. Although of a small magnitude, the upregulation of GFAP immunoreactivity was already significant in the thalamus and cortex of 1 month old *Cln5*$^{-/-}$ mice (Figure 5), and became more pronounced with increased age, especially within the thalamus.

Microglial activation—Before 12 months of age, there were no discernable differences between genotypes in the extent and distribution of F4/80 immunoreactivity, but staining for this marker revealed pronounced and localized microglial activation in 12 month old *Cln5*$^{-/-}$ mice (Figure 6). At all ages control mice displayed widespread distribution of ramified microglia in the S1BF (Figure 6A) and V1 (Figure 6C), revealed by pale F4/80 immunoreactivity. In contrast, a higher level of microglial activation was seen in both S1BF and V1 of *Cln5*$^{-/-}$ mice, with intensely F4/80 immunoreactive microglia predominantly within deeper laminae, with occasional darkly stained microglia in more superficial laminae (Figure 6A, 6C). Compared to the palely stained and highly ramified microglia evident in the cortex

of control mice (Figure 6A, 6C), microglia in *Cln5* deficient mice displayed a larger more intensely stained soma with numerous short bushy processes. Differences between genotypes in the relative intensity of F4/80 immunoreactivity and microglial morphology were more prominent in subcortical structures (Figure 6C and 6D). 12 month old *Cln5*$^{-/-}$ mice displayed localized microglial activation within individual thalamic nuclei (Figure 6B, 6D), in contrast to widespread distribution of palely stained microglia in age-matched littermate controls. Morphologically, many of the intensely stained microglia in mutant mice displayed an enlarged soma and short thickened processes typical of an amoeboid or brain macrophage like appearance (Figure 6D), versus the less intensely stained microglia with thin ramified processes present in age-matched controls. This dramatic upregulation of F4/80 immunoreactivity was confirmed by thresholding image analysis revealing significantly increased microglial activation in the both S1BF and VPM/VPL in 12 month old *Cln5* deficient mice (Figure 6E).

Late onset thalamic relay neuron loss in *Cln5* deficient mice

In other forms of NCL the thalamic nuclei that exhibit localized astrocytosis, subsequently display neuron loss several months before neurons in their corresponding cortical target regions (Kielar et al., 2007). To investigate whether *Cln5*$^{-/-}$ mice displayed a similar relationship between thalamic and cortical neuron loss we used unbiased stereology to determine the extent of neuronal loss in Nissl stained sections within three thalamic nuclei (Figure 7) that relay different sensory modalities to the cortex (somatosensory, ventral posterior thalamic nucleus VPM/VPL; visual, dorsal lateral geniculate nucleus LGNd; auditory, medial geniculate nucleus MGN). Optical fractionator estimates of neuron number in *Cln5* deficient mice revealed selective effects upon thalamic relay neuron survival that occurred relatively late in disease progression. There was a significant loss of VPM/VPL and LGNd neurons in *Cln5*$^{-/-}$ mice that only became evident at 12 months of age, but no significant loss of MGN neurons even in these aged mutant mice (Figure 7A).

Early onset cortical neuron loss in *Cln5* deficient mice

Since these changes in thalamic neuron number only became evident once cortical atrophy was apparent, we next investigated the relative timing of cortical neuron loss in *Cln5* mutant mice and age-matched controls at 4 and 12 months of age. We focussed our analysis upon S1BF and V1, the cortical target regions of the two thalamic relay nuclei (VPM/VPL and LGNd respectively), which displayed significant neuron loss at 12 months. To do this we obtained optical fractionator estimates in mice of both genotypes of the number of Nissl stained granule neurons in lamina IV granule neurons that receive thalamic innervation, lamina VI neurons that supply feedback to the thalamus, and lamina V projection neurons (Figure 7B, 7C).

Surprisingly, this analysis revealed a relatively early and significant loss of cortical neurons in *Cln5* deficient mice at 4 months of age, which became more widespread and involved more laminae with increased age. Although present in both cortical regions of *Cln5*$^{-/-}$ mice, this neuron loss was more pronounced and occurred earlier within the visual system with significant effects upon the number of lamina IV granule neurons and lamina V projection neurons in V1 already evident at 4 months of age (Figure 7C). In contrast, the somatosensory cortex was better preserved at this age with significant neuron loss only present in lamina V of S1BF at 4 months of age, with a significant loss of lamina IV neurons also observed in *Cln5* mutant mice at 12 months of age (Figure 7B).

This relatively early onset of cortical neuron loss in *Cln5* mutant mice is in marked contrast to our findings in mouse models of other forms of NCL (Weimer et al., 2006; Kielar et al., 2007; Partanen et al., 2008). To provide a direct comparison to another NCL mouse model that was raised on the same mixed background and housed in the same animal house, we next surveyed thalamocortical neuron survival in *Ppt*$^{\Delta ex4}$ mice, a knock-in model of *Cln1* deficiency

(Jalanko et al., 2005). In contrast to *Cln5*$^{-/-}$ mice, optical fractionator estimates in *Ppt*$^{\Delta ex4}$ mice revealed a significant loss of thalamic relay neurons in both VPM/VPL and LGNd that was already evident at 4 months of age, but with no effects upon cortical neuron survival in these mice at this age (Figure 8). These data not only confirm our previous findings in another mouse model of INCL (Kielar et al., 2007), but emphasize the unexpected nature of our findings in *Cln5* deficient mice, which display a completely reversed sequence of neuron loss occurring first within the cortex and only subsequently in the thalamus (Figures 7 and 9).

Discussion

Characterization of NCL mouse models is revealing a wealth of new information about disease progression and this study provides the first detailed description of the sequence of pathological events in *Cln5*$^{-/-}$ mice. As in mouse models of other forms of NCL, the thalamocortical system of these *Cln5* deficient mice displayed localized reactive changes and progressive neuron loss that became more pronounced with increased age. However, in marked contrast to all other forms of NCL characterized to date (Figure 9), neuron loss in *Cln5*$^{-/-}$ mice began in the cortex and only subsequently occurred in the corresponding thalamic relay nuclei. These surprising data reveal that neuron loss in *Cln5*$^{-/-}$ mice progresses through the thalamocortical pathways in the opposite direction to that seen previously in all other forms of NCL.

Common themes in NCL pathogenesis?

The recent availability of mouse models for seven different forms of NCL has seen a series of studies describing the pathological phenotype of each disease model (reviewed by Cooper et al., 2006). Phenotypically these mice resemble the human disorder, displaying accumulation of autofluorescent storage material, profound astrocytosis and microglial activation, widespread neuron loss and brain atrophy (Cooper et al., 1999; Mitchison et al., 1999; Bible et al., 2004; Kopra et al., 2004; Pontikis et al., 2004, 2005; Sleat et al., 2004; Jalanko et al., 2005; Kielar et al., 2007; Partanen et al., 2008). Our data from 12 month old *Cln5* deficient mice reveal a similar phenotype with widespread regional atrophy and generalized thinning of the cortex (Figure 1), pronounced astrocytosis and microglial activation that are most pronounced within the thalamocortical system (Figures 4 and 6). Coming at the end of a late onset and slowly progressing NCL-like disorder, this phenotype closely resembles that of *Cln3* mutant models of juvenile NCL (JNCL) (Mitchison et al., 1999; Cotman et al., 2002; Pontikis et al., 2004, 2005). This is in contrast to much earlier onset and rapidly progressing degenerative phenotypes of mouse models of infantile (Gupta et al., 2002; Jalanko et al., 2005; Kielar et al., 2007), and especially congenital NCL (Partanen et al., 2008), suggesting a correlation between disease severity in these models and the corresponding human condition. However, as our findings in *Cln5* deficient mice highlight, although these mouse models display similar pathological endpoints (Mitchison et al., 2004; Cooper et al., 2006), these may be preceded by a sequence of neuron loss within thalamocortical pathways that progresses differently between forms of NCL. Indeed, it is only by systematically studying the staging of these disorders that such important differences can become apparent.

Until recently, the cortex has long been considered the main pathological target in multiple forms of NCL, exhibiting profound atrophy and severe neuron loss at autopsy (Haltia 2003). However, it is now emerging that the thalamus is consistently affected early in disease progression (Autti et al., 1997, 2007), with an early loss of thalamic relay neurons before the degeneration starts in the corresponding cortical region. This phenotype is shared by multiple models of JNCL (Pontikis et al., 2005; Weimer et al., 2006), Infantile (Kielar et al., 2007; Figure 8) and Congenital NCL (Partanen et al., 2008) and similar data are emerging in the remaining forms of variant late infantile NCL (Cooper and Wong, unpublished observations). Indeed, these are robust phenotypes that persist across different strain backgrounds and

different targeting strategies used to disrupt each gene, leading to the suggestion that this is a central feature to NCL pathogenesis.

Distinctive features of *Cln5* deficiency

Given the consistency of this early thalamic involvement, our data from *Cln5* deficient mice are particularly surprising, revealing that these events occur in a completely reversed order in *Cln5*$^{-/-}$ mice (Figures 7 and 9), with neuron loss starting in the cortex and only subsequently occurring in the thalamus. Although the *Cln5* deficient mice used in this study were upon a mixed strain background, the phenotype of *Ppt1*$^{\Delta ex4}$ knock-in mice on the same background (Jalanko et al., 2005 and Figure 8), and housed in the same animal facility exhibit a phenotype remarkably similar to that of *Ppt1*$^{-/-}$ deficient mice on a congenic background (Kielar et al., 2007). Indeed our findings from both INCL and JNCL mouse models reveals very little difference between the NCL phenotypes of these mice upon mixed strain or different congenic mouse strains (Bible et al., 2004; Pontikis et al., 2004, 2005; Kielar et al., 2007; Cooper and Pearce, unpublished observations).

Despite the fundamental difference in their relative timing of cortical and thalamic neuron loss (Figure 9), one consistent feature of NCL pathogenesis that is retained in *Cln5*$^{-/-}$ mice is the early targeting of the visual system. For example, visual relay neurons are lost before somatosensory relay neurons in *Cln3* and *Ppt1* null mutant mice (Weimer et al., 2006;Kielar et al., 2007), and in *Ppt1*$^{\Delta ex4}$ mice LGNd neurons are also lost early in disease progression (Figure 8). Indeed, such early loss of visual relay neurons, suggests that visual failure is due to pathological effects on central visual pathways rather than solely retinal degeneration (Weimer et al., 2006). Changes in the expression of several genes that play important roles within the visual system are evident in *Cln5* deficient mice (von Schantz et al 2008). Moreover, the onset of neuron loss in the primary visual cortex in these *Cln5* deficient mice (Figure 7) coincides with the onset of visual failure in these mice (Kopra et al., 2004). Although the basis of visual dysfunction in these mice remains unclear, it will be important to define the relationship between neuron loss within the retina and more central components of the visual system in *Cln5*$^{-/-}$ mice.

Although astrocytosis has long been considered a hallmark of neurodegenerative changes, it is now apparent that glial responses often precede neuron loss and may be indicative of neuronal dysfunction (Raivich et al., 1999). Indeed, the early glial responses that occur in multiple forms of NCL and other LSDs accurately predict where neuron loss subsequently occurs (Oswald et al., 2005; Kielar et al., 2007; reviewed by Castañeda et al., 2008). In this respect the presence of early and localized astrocytosis within the thalamus of *Cln5*$^{-/-}$ mice (Figure 4) is not surprising, but its precise staging and relationship to neuron loss is unusual and emphasizes the different nature of these events between forms of NCL. Given the relatively slow neurological phenotype of *Cln5* deficient mice (Kopra et al., 2004), and the late onset of thalamic neuron loss (Figure 7), this astrocytosis occurs remarkably early in pathogenesis and may reflect a combination of several ongoing pathological events which lead ultimately to neuron loss. These may include dendritic, afferent axonal or synaptic pathologies which occur in other forms of NCL (e.g. Partanen et al., 2008), and it will be important to discover the precise relationship between these events and neuron loss in *Cln5* deficient mice. In contrast, microglial activation in *Cln5*$^{-/-}$ mice follows a more predictable course and is most pronounced in the later stages of disease progression, as previously reported in *Ppt1*$^{-/-}$ mice (Kielar et al., 2007). This microglial activation was most pronounced in the thalamus of *Cln5* deficient mice (Figure 6), with the transformation of microglia to brain macrophage like morphology also most pronounced in the thalamus. This may reflect that neuron loss is still ongoing in both LGNd and VPM/VPL (Figure 6), but is effectively complete in V1 and S1BF with no pronounced increase in neuron loss above that seen at 4 months of age (Figure 7).

The reason for the distinctive and unexpected thalamocortical phenotype of *Cln5* deficient mice is not presently clear. As we have reported previously, *Cln5* deficient mice display widespread and indiscriminate accumulation of storage material through out the brain, with no detectable differences between brain regions or cortical laminae (Kopra et al., 2004). Elevated levels of storage material are evident as early as one month of age and can be seen by electron microscopy in both cortical and thalamic neurons at three months of age (Kopra et al., 2004). However, as in models of other forms of NCL (Bible et al., 2004; Oswald et al., 2005; Kielar et al., 2007), there is no direct correlation between the timing or distribution of storage material accumulation in *Cln5*$^{-/-}$ mice (Kopra et al., 2004), and the distinctive pattern of neuron loss we have revealed in these mice. Moreover, Cln5 and Ppt1 display remarkably similar CNS expression profiles (Heinonen et al., 2000), which also do not explain the contrasting cortical *vs.* thalamic initiation of neuron loss evident in *Cln5*$^{-/-}$ and *Ppt1*$^{\Delta ex4}$ mice, respectively. Indeed, even though gene expression profiling has implied that the same cellular pathways are affected in both *Ppt1* and *Cln5* deficient mice (von Schantz et al., 2008), it is apparent that the consequences of mutations in *Cln5* are radically different in the thalamocortical system.

There is a prominent involvement of synaptic pathology in both *Ppt1* and *Cathepsin D* deficient mice (Partanen et al., 2008; Kim et al., 2008), which is particularly pronounced within the thalamus (Partanen et al., 2008; Kielar, Gillingwater and Cooper, unpublished observations). This synaptic phenotype correlates with the early loss of loss of thalamic relay neurons in these mouse models (Kielar et al., 2007; Partanen et al., 2008). Our data provide the first evidence for synaptic pathologies in this form of NCL, with pronounced differences in the staining for a series of presynaptic markers in severely affected *Cln5* deficient mice (Figure 3). Although synaptophysin and VAMP2 displayed similar trends in the cortex and thalamus of mutant mice, staining for SNAP25 was affected differently between these regions (Figure 3), hinting that dissimilar pathological events happening in the thalamus and cortex of *Cln5* deficient mice. It will be important to determine the relationship between these synaptic pathologies and the distinctive sequence of neuron that occurs in the thalamocortical system of these *Cln5*$^{-/-}$ mice.

Implications for therapy?

The characteristic and unexpected pattern of neuron loss in *Cln5* deficient mice highlights the need to determine the mechanisms that underlie neuron vulnerability in these disorders. However, regardless of the underlying mechanism, the discovery of cortical rather than thalamic predominance in vLINCL$_{Fin}$ pathogenesis has important implications for the targeting of therapies for this disorder. Indeed, if therapies are to be delivered to where and when they can be most effective, these data highlight the need to study the progressive pathological changes that lead up to the end stages of any disease. This is particularly relevant for vLINCL$_{Fin}$ since the *CLN5/Cln5* gene product has now been identified as a soluble lysosomal glycoprotein that appears to be trafficked via the mannose-6-phosphate pathway (Holmberg et al 2004; Sleat et al., 2005). This discovery implies that cross-correction of *Cln5* deficient neurons is possible, paving the way for gene therapy approaches that will be most likely to succeed if targeted to where pathology is first apparent. In this respect our findings from *Cln5*$^{-/-}$ mice are likely to be particularly informative and the recent confirmation of a large animal model of *CLN5* deficiency (Frugier et al., 2008), provides an ideal opportunity to test methods for the effective delivery of appropriately targeted therapy in this profoundly disabling disorder.

Acknowledgments

These studies were supported by National Institutes of Health grant NS41930 (JDC) and European Commission 6th Framework Research Grant LSHM-CT-2003-503051 (JDC, AJ) and Academy of Finland, Centre of Excellence in Complex Disease Genetics Grant 213506 (AJ). The following non-profit agencies also contributed financially to this work: The Batten Disease Support and Research Association (JDC, CK), The Natalie Fund (JDC), The Batten Disease

Family Association (JDC, CK) and the Remy Fund (JDC), The Sigrid Juselius Foundation (AJ), the Finnish Cultural Foundation (CVSF) and the Helsinki Graduate School in Biotechnology and Molecular Biology (CVSF). We would like to thank the other members of the PSDL and the Department of Molecular Medicine for their valuable contributions: Drs. Thomas Gillingwater, Andrew Wong and Alison Barnwell for constructive comments on the manuscript.

References cited

Autti T, Raininko R, Santavuori P, Vanhanen SL, Poutanen VP, Haltia M. MRI of neuronal ceroid lipofuscinosis. II. Postmortem MRI and histopathological study of the brain in 16 cases of neuronal ceroid lipofuscinosis of juvenile or late infantile type. Neuroradiology 1997;39:371–377. [PubMed: 9189886]

Autti T, Joensuu R, Aberg L. Decreased T2 signal in the thalami may be a sign of lysosomal storage disease. Neuroradiology 2007;49:571–578. [PubMed: 17334752]

Bible E, Gupta P, Hofmann SL, Cooper JD. Regional and cellular neuropathology in the palmitoyl protein thioesterase-1 (PPT1) null mutant mouse model of infantile neuronal ceroid lipofuscinosis. Neurobiol Dis 2004;16:346–359. [PubMed: 15193291]

Castañeda JA, Lim MJ, Cooper JD, Pearce DA. Immune system irregularities in lysosomal storage disorders. Acta Neuropathol 2008;115:159–174. [PubMed: 17924126]

Cooper JD. Progress towards understanding the neurobiology of Batten disease or neuronal ceroid lipofuscinosis. Curr Opin Neurol 2003;16:121–128. [PubMed: 12644737]

Cooper JD, Messer A, Feng AK, Chua-Couzens J, Mobley WC. Apparent loss and hypertrophy of interneurons in a mouse model of neuronal ceroid lipofuscinosis: evidence for partial response to insulin-like growth factor-1 treatment. J Neurosci 1999;19:2556–2567. [PubMed: 10087069]

Cooper JD, Russell C, Mitchison HM. Progress towards understanding disease mechanisms in small vertebrate models of neuronal ceroid lipofuscinosis. Biochim Biophys Acta 2006;1762:873–89. [PubMed: 17023146]

Cotman SL, Vrbanac V, Lebel LA, Lee RL, Johnson KA, Donahue LR, Teed AM, Antonellis K, Bronson RT, Lerner TJ, MacDonald ME. *Cln3*$^{\Delta ex7/8}$ knock-in mice with the common JNCL mutation exhibit progressive neurologic disease that begins before birth. Hum Mol Genet 2002;11:2709–2721. [PubMed: 12374761]

Frugier T, Mitchell NL, Tammen I, Houweling PJ, Arthur DG, Kay GW, van Diggelen OP, Jolly RD, Palmer DN. A new large animal model of CLN5 neuronal ceroid lipofuscinosis in Borderdale sheep is caused by a nucleotide substitution at a consensus splice site (c.571+1G>A) leading to excision of exon 3. Neurobiol Dis 2008;29:306–315. [PubMed: 17988881]

Gundersen HJ, Jensen EB. The efficiency of systematic sampling in stereology and its prediction. J Microsc 1987;147:229–263. [PubMed: 3430576]

Gupta P, Soyombo AA, Atashband A, Wisniewski KE, Shelton JM, Richardson JA, Hammer RE, Hofmann SL. Disruption of PPT1 or PPT2 causes neuronal ceroid lipofuscinosis in knockout mice. Proc Natl Acad Sci USA 2001;98:13566–13571. [PubMed: 11717424]

Haltia M. The neuronal ceroid-lipofuscinoses. J Neuropathol Exp Neurol 2003;62:1–13. [PubMed: 12528813]

Heinonen O, Salonen T, Jalanko A, Peltonen L, Copp A. CLN-1 and CLN-5, genes for infantile and variant late infantile neuronal ceroid lipofuscinoses, are expressed in the embryonic human brain. J Comp Neurol 2000;426:406–412. [PubMed: 10992246]

Isosomppi J, Vesa J, Jalanko A, Peltonen L. Lysosomal localization of the neuronal ceroid lipofuscinosis CLN5 protein. Hum Mol Genet 2002;11:885–891. [PubMed: 11971870]

Jalanko A, Vesa J, Manninen T, von Schantz C, Minye H, Fabritius AL, Salonen T, Rapola J, Gentile M, Kopra O, Peltonen L. Mice with *Ppt1*$^{\Delta ex4}$ mutation replicate the INCL phenotype and show an inflammation-associated loss of interneurons. Neurobiol Dis 2005;18:226–241. [PubMed: 15649713]

Kielar C, Maddox L, Bible E, Pontikis CC, McCauley SL, Griffey MA, Wong M, Sands MS, Cooper JD. Successive neuron loss in the thalamus and cortex in a mouse model of infantile neuronal ceroid lipofuscinosis. Neurobiol Dis 2007;25:150–162. [PubMed: 17046272]

Kim SJ, Zhang Z, Sarkar C, Tsai PC, Lee YC, Dye L, Mukherjee AB. Palmitoyl protein thioesterase-1 deficiency impairs synaptic vesicle recycling at nerve terminals, contributing to neuropathology in humans and mice. J Clin Invest 2008;118:3075–3086. [PubMed: 18704195]

Kopra O, Vesa J, von Schantz C, Manninen T, Minye H, Fabritius AL, Rapola J, van Diggelen OP, Saarela J, Jalanko A, Peltonen L. A mouse model for Finnish variant late infantile neuronal ceroid lipofuscinosis, CLN5, reveals neuropathology associated with early aging. Hum Mol Genet 2004;13:2893–2906. [PubMed: 15459177]

Mole SE, Williams RE, Goebel HH. Correlations between genotype, ultrastructural morphology and clinical phenotype in the neuronal ceroid lipofuscinoses. Neurogenetics 2005;6:107–126. [PubMed: 15965709]

Mitchison HM, Bernard DJ, Greene NDE, Cooper JD, Junaid MA, Pullarkat RK, Vos N, Breuning MH, Owens JW, Mobley WC, Gardiner RM, Lake BD, Taschner PEM, Nussbaum RL. Targeted Disruption of the Cln3 gene provides a mouse model for Batten Disease. The Batten Mouse Model Consortium. Neurobiol Dis 1999;6:321–334. [PubMed: 10527801]

Oswald MJ, Palmer DN, Kay GW, Shemilt SJA, Rezaie P, Cooper JD. Glial activation spreads from specific cerebral foci and precedes neurodegeneration in presymptomatic ovine neuronal ceroid lipofuscinosis (CLN6). Neurobiol Dis 2005;20:49–63. [PubMed: 16137566]

Partanen S, Haapanen A, Kielar C, Pontikis C, Alexander N, Inkinen T, Saftig P, Gillingwater TH, Cooper JD, Tyynelä J. Synaptic changes in the thalamocortical system of cathepsin D-deficient mice: a model of human congenital neuronal ceroid-lipofuscinosis. J Neuropathol Exp Neurol 2008;67:16–29. [PubMed: 18091563]

Paxinos, G.; Franklin, KBJ. The mouse brain in stereotaxic coordinates. Vol. Second. Academic Press; San Diego: 2001.

Pontikis CC, Cella CV, Parihar N, Lim MJ, Chakrabarti S, Mitchison HM, Mobley WC, Rezaie P, Pearce DA, Cooper JD. Late onset neurodegeneration in the *Cln3*$^{-/-}$ mouse model of juvenile neuronal ceroid lipofuscinosis is preceded by low level glial activation. Brain Res 2004;1023:231–242. [PubMed: 15374749]

Pontikis CC, Cotman SL, MacDonald ME, Cooper JD. Thalamocortical neuron loss and localized astrocytosis in the *Cln3*$^{\Delta ex7/8}$ knock-in mouse model of Batten disease. Neurobiol Dis 2005;20:823–836. [PubMed: 16006136]

Raivich G, Bohatschek M, Kloss CU, Werner A, Jones LL, Kreutzberg GW. Neuroglial activation repertoire in the injured brain: graded response, molecular mechanisms and cues to physiological function. Brain Res 1999;30:77–105.

Santavuori P, Rapola J, Sainio K, Raitta C. A variant of Jansky-Bielschowsky disease. Neuropediatrics 1982;13:135–141. [PubMed: 7133332]

Santavuori P. Neuronal ceroid-lipofuscinoses in childhood. Brain Dev 1988;10:80–83. [PubMed: 3291628]

Santavuori P, Rapola J, Raininko R, Autti T, Lappi M, Nuutila A, Launes J, Sainio K. Early juvenile neuronal ceroid-lipofuscinosis or variant Jansky-Bielschowsky disease: diagnostic criteria and nomenclature. J Inherit Metab Dis 1993;16:230–232. [PubMed: 8411967]

Siintola E, Lehesjoki AE, Mole SE. Molecular genetics of the NCLs -- status and perspectives. Biochim Biophys Acta 2006;1762:857–864. [PubMed: 16828266]

Siintola E, Topcu M, Aula N, Lohi H, Minassian BA, Paterson AD, Liu XQ, Wilson C, Lahtinen U, Anttonen AK, Lehesjoki AE. The novel neuronal ceroid lipofuscinosis gene MFSD8 encodes a putative lysosomal transporter. Am J Hum Genet 2007;81:136–146. [PubMed: 17564970]

Sleat DE, Wiseman JA, El-Banna M, Kim KH, Mao Q, Price S, Macauley SL, Sidman RL, Shen MM, Zhao Q, Passini MA, Davidson BL, Stewart GR, Lobel P. A mouse model of classical late-infantile neuronal ceroid lipofuscinosis based on targeted disruption of the CLN2 gene results in a loss of tripeptidyl-peptidase I activity and progressive neurodegeneration. J Neurosci 2004;24:9117–9126. [PubMed: 15483130]

Sleat DE, Lackland H, Wang Y, Sohar I, Xiao G, Li H, Lobel P. The human brain mannose 6-phosphate glycoproteome: a complex mixture composed of multiple isoforms of many soluble lysosomal proteins. Proteomics 2005;5:1520–1532. [PubMed: 15789345]

Tyynelä J, Cooper JD, Khan MN, Shemilt SJA, Haltia M. Specific Patterns of Storage Deposition, Neurodegeneration, and Glial Activation in the Hippocampus of Patients with Neuronal Ceroid-Lipofuscinoses. Brain Pathol 2004;14:349–357. [PubMed: 15605981]

Vesa J, Chin MH, Oelgeschlager K, Isosomppi J, DellAngelica EC, Jalanko A, Peltonen L. Neuronal ceroid lipofuscinoses are connected at molecular level: interaction of CLN5 protein with CLN2 and CLN3. Mol Biol Cell 2002;13:2410–2420. [PubMed: 12134079]

von Eitzen U, Egensperger R, Kosel S, Grasbon-Frodl EM, Imai Y, Bise K, Kohsaka S, Mehraein P, Graeber MB. Microglia and the development of spongiform change in Creutzfeldt-Jakob disease. J Neuropathol Exp Neurol 1998;57:246–256. [PubMed: 9600217]

von Schantz C, Saharinen J, Kopra O, Cooper JD, Gentile M, Hovatta I, Peltonen L, Jalanko A. Brain gene expression profiles of Cln1 and Cln5 deficient mice unravels common molecular pathways underlying neuronal degeneration in NCL diseases. BMC Genomics 2008;9:146. [PubMed: 18371231]

Weimer JM, Custer AW, Benedict JW, Alexander NA, Kingsley E, Federoff HJ, Cooper JD, Pearce DA. Visual deficits in a mouse model of Batten disease are the result of optic nerve degeneration and loss of dorsal lateral geniculate thalamic neurons. Neurobiol Dis 2006;22:284–293. [PubMed: 16412658]

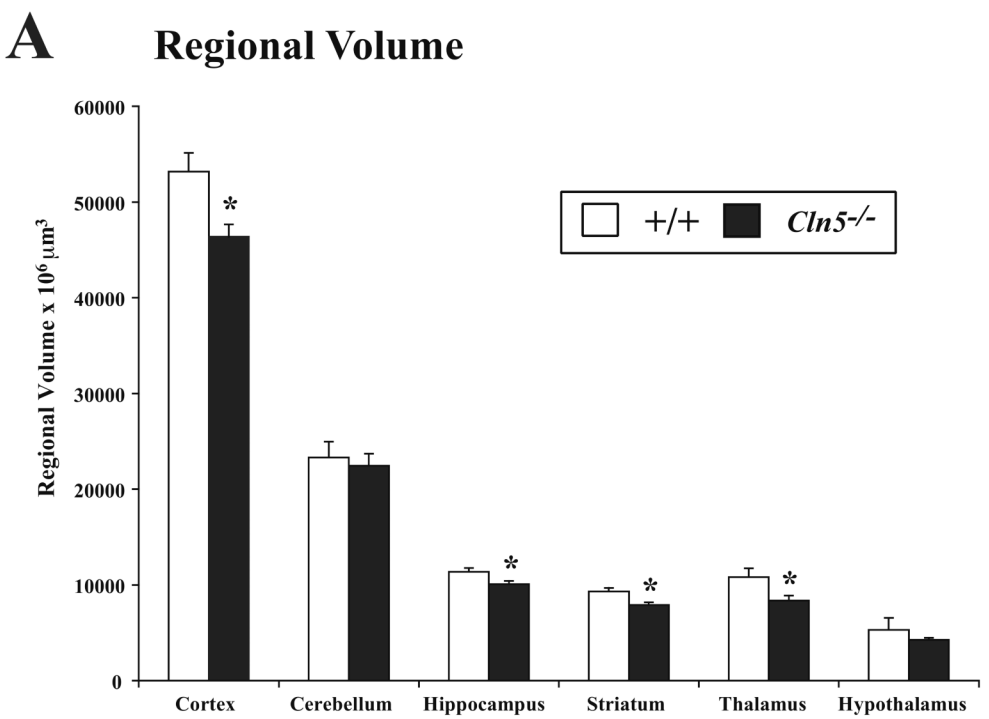

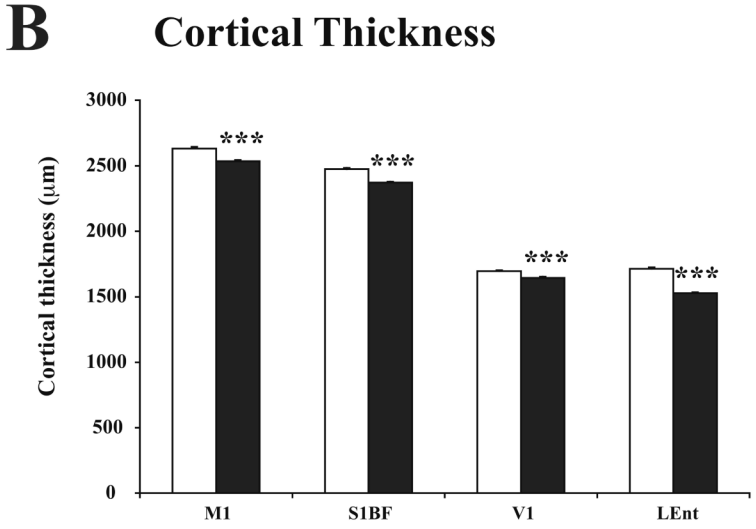

Figure 1.

Regional atrophy and cortical thinning in *Cln5* deficient mice. (A) Unbiased Cavalieri estimates of regional volume revealed significant atrophy of the cortex, hippocampus, striatum and thalamus in 12 month old *Cln5* deficient mice (*Cln5*$^{-/-}$) *vs.* littermate controls (+/+). In contrast, the cerebellum and hypothalamus did not exhibit significant reduction in volume in mutant mice (mean±SEM; * $p<0.05$; ANOVA with post-hoc Bonferroni analysis). (B) Cortical thickness measurements of primary motor (M1), primary somatosensory (S1BF), primary visual (V1) and lateral entorhinal (LEnt) cortex revealed a significant thinning of these cortical regions in 12 month old *Cln5*$^{-/-}$ mice *vs.* littermate controls (mean±SEM; *** $p<0.001$; ANOVA with post-hoc Bonferroni analysis).

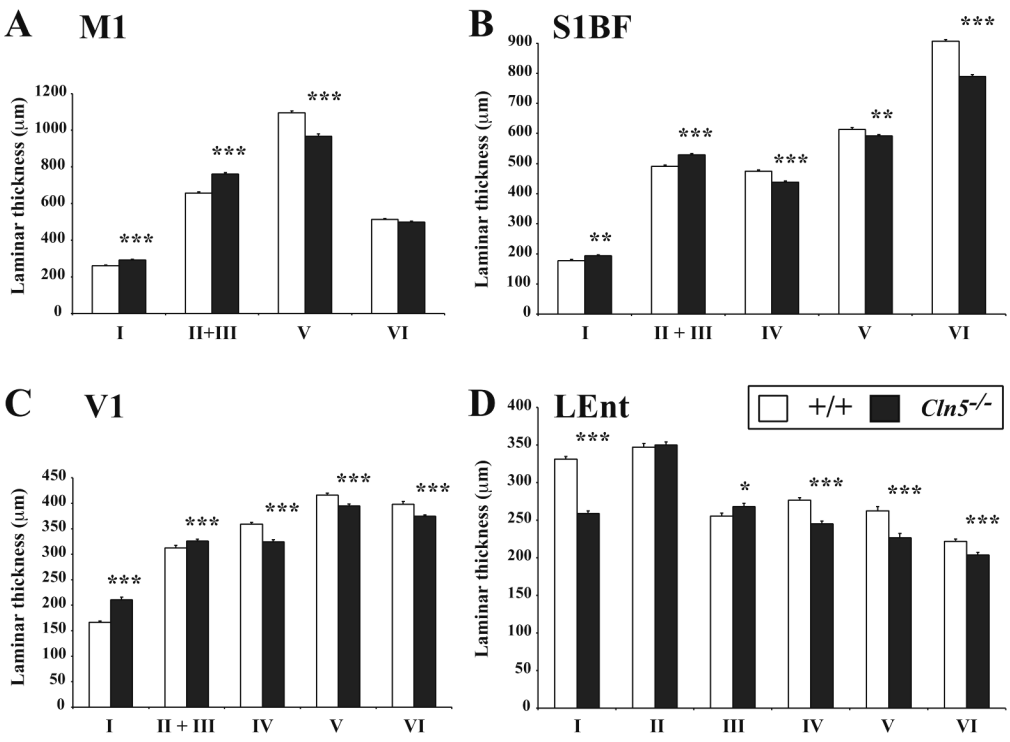

Figure 2.

Widespread laminar specific effects upon the cortical mantle of *Cln5* deficient mice. **(A-D)** Laminar thickness measurements in primary motor (M1, A), primary somatosensory (S1BF, B), primary visual (V1, C) and lateral entorhinal (LEnt, D) cortex revealed a complex series of changes in the thickness of individual laminae in 12 month old *Cln5*$^{-/-}$ mice compared with littermate controls. Consistent across all cortical regions mutant mice displayed significant thinning of the deeper laminae (IV-VI), but a trend towards increased thickness in more superficial laminae (I-III) that was less pronounced in LEnt. (mean±SEM; * $p<0.05$; ** $p<0.01$; *** $p<0.001$; ANOVA with post-hoc Bonferroni analysis).

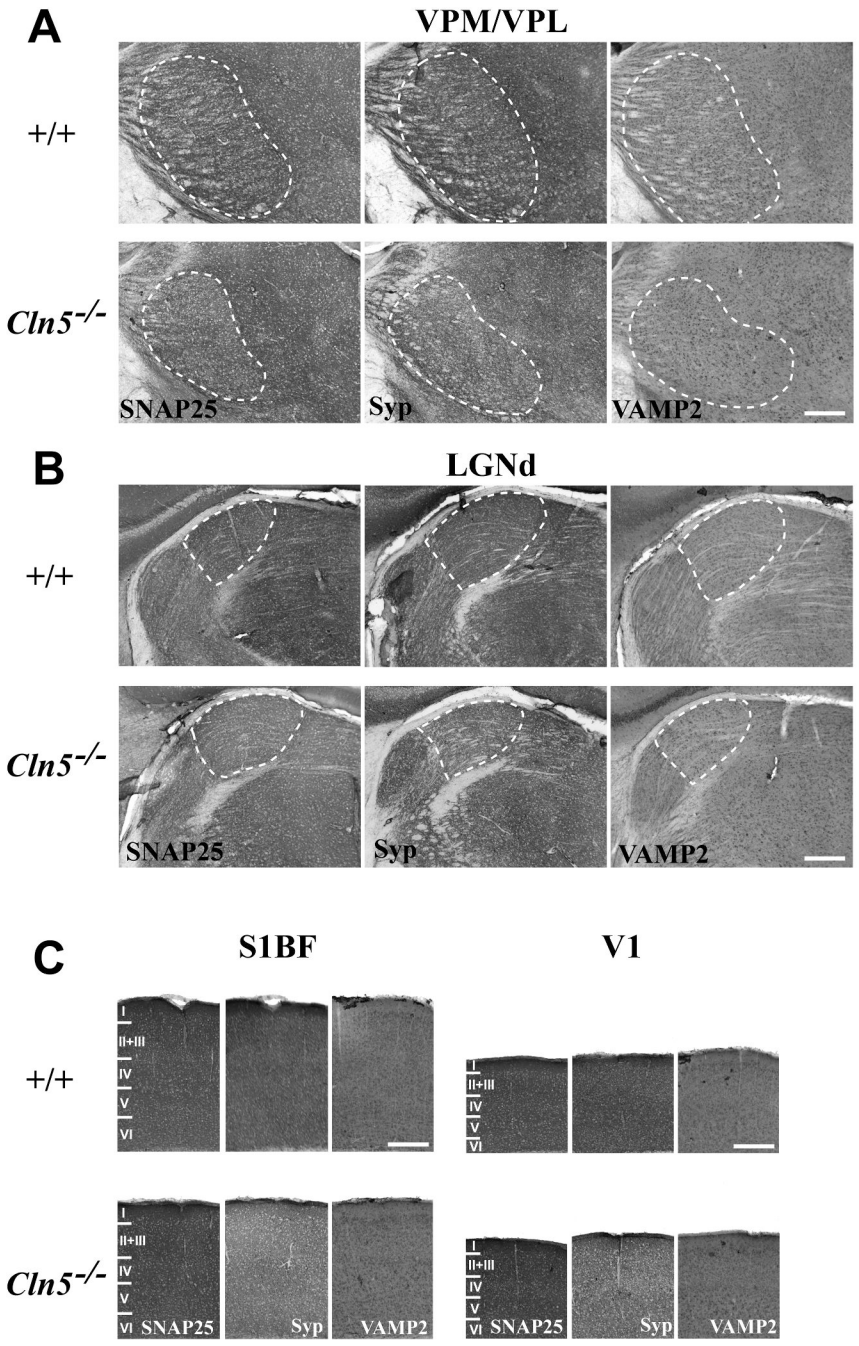

Figure 3.

Altered expression of presynaptic markers in the visual and somatosensory system of *Cln5* deficient mice. Immunohistochemical staining for the SNARE complex protein SNAP25, the pre-synaptic membrane protein synaptophysin (Syp), and the synaptic vesicle protein synaptobrevin (VAMP2) reveal altered intensity and distribution of these presynaptic markers in the thalamocortical system of 12 month old *Cln5* deficient mice (*Cln5*$^{-/-}$) compared with age-matched control mice (+/+). (A) Within the somatosensory (ventral posterior, VPM/VPL) thalamic relay nucleus, severely affected *Cln5* mice displayed reduced staining intensity for both SNAP25 and Syp, but relatively little change in these markers in adjacent nuclei. In contrast VAMP2 was generally increased in clusters around persisting VPM/VPL neurons. (B)

A similar phenotype was evident in the visual (dorsal lateral geniculate, LGNd) relay nucleus of the thalamus, with reduced SNAP25 and Syp immunoreactivty, and the redistribution of VAMP2 immunoreactivity around surviving LGNd neurons. (C) In the primary somatosensory barrelfield (S1BF) and primary visual cortex (V1) of 12 month old Cln5reduced staining for Syp and redistribution of VAMP2 were also evident. However, unlike either VPM/VPL and LGNd, staining for SNAP25 was relatively preserved in both S1BF and V1 of these severely affected mutant mice. The boundaries of thalamic nuclei are indicated by white dashed lines and cortical laminae with roman numerals. Scale bar = 300μm.

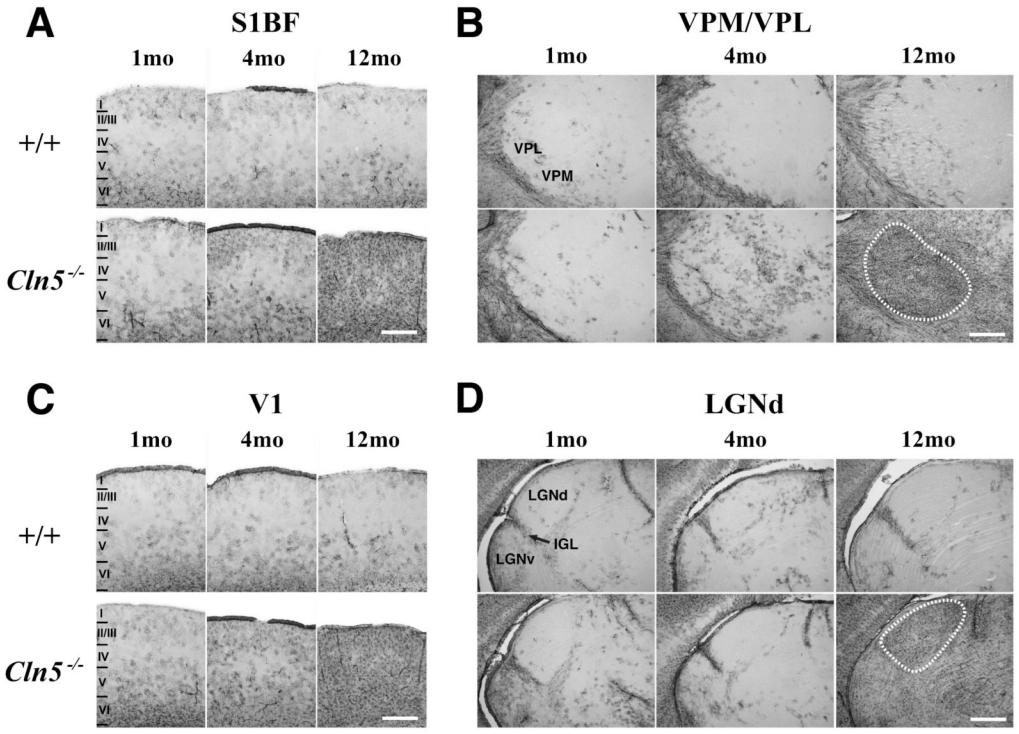

Figure 4.

Progressive astrocytosis in the thalamocortical system of *Cln5* deficient mice. **(A-D)** Immunohistochemical staining for glial fibrillary associated protein (GFAP) reveals the pronounced upregulation of this marker of astrocytosis with increased age in the somatosensory barrelfield cortex (S1BF, A) primary visual cortex (V1, C) of *Cln5*$^{-/-}$ mice compared to age matched controls (+/+). **(A, C)** At one month of age only few scattered GFAP immunoreactive astrocytes were evident mostly in deeper laminae of both S1BF and V1 in control mice, with similar staining evident in *Cln5*$^{-/-}$ mice. In these mutant mice at 4 months of age GFAP immunoreactivity became more pronounced in both deeper laminae (IV-VI) and superficial laminae (I-III) of both cortical regions, becoming markedly more intense and spreading to involve all laminae at 12 months of age. Laminar boundaries are indicated by roman numerals. **(B, D)** A similar progressive increase in the distribution and intensity of GFAP immunoreactivity was also evident in the ventral posterior (VPM/VPL, B) and dorsal lateral geniculate (LGNd, D) thalamic nucleus, which project to S1BF and V1, respectively. At 1 month of age GFAP immunoreactivity appeared similar in control and *Cln5*$^{-/-}$ mice, but numerous scattered GFAP-positive astrocytes were evident in VPM/VPL at 4 months of age. In contrast LGNd contained few GFAP immunoreactive astrocytes until 12 months of age when intense GFAP staining delineated both VPM/VPL and LGNd. The boundaries of these nuclei are indicated by white dashed lines. Scale bar = 300 μm.

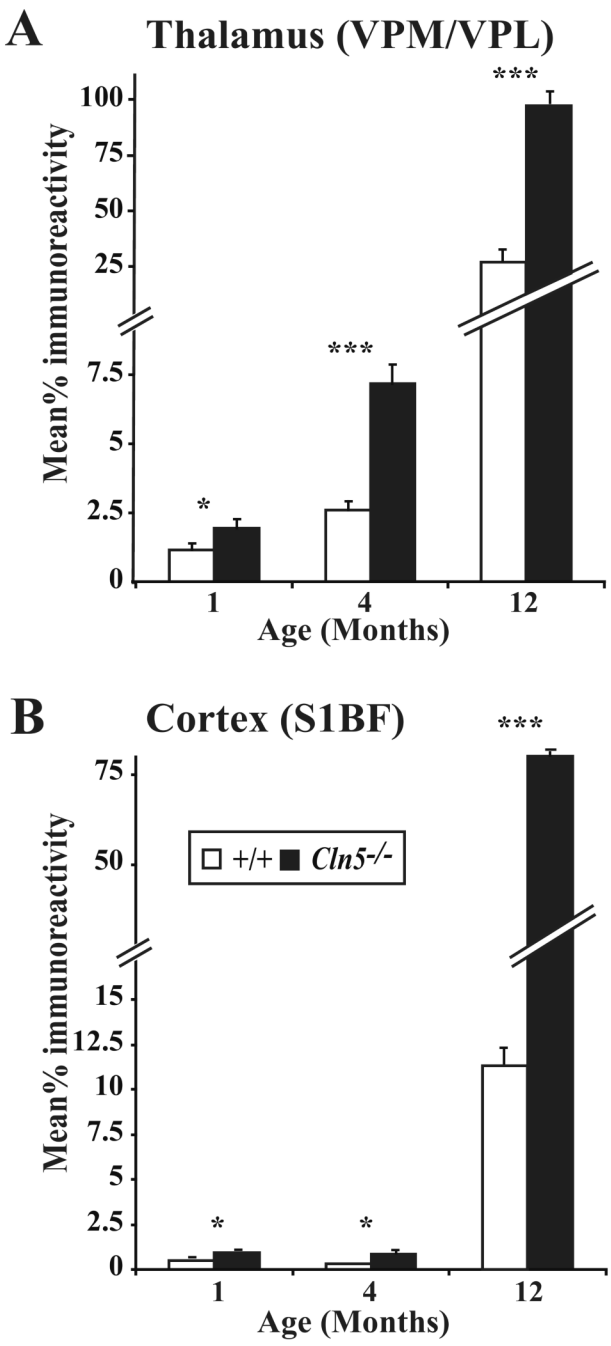

Figure 5.

Increased astrocytosis with disease progression in *Cln5* deficient mice **(A, B)** Thresholding image analysis confirms the progressive and significant accumulation of GFAP staining in both the thalamus (***VPM/VPL***, A) and cortex (***S1BF***, B) of *Cln5* deficient mice (*Cln5*$^{-/-}$) with increased age, compared to age matched controls (+/+). (mean±SEM; * $p<0.05$; *** $p<0.001$; ANOVA with post-hoc Bonferroni analysis).

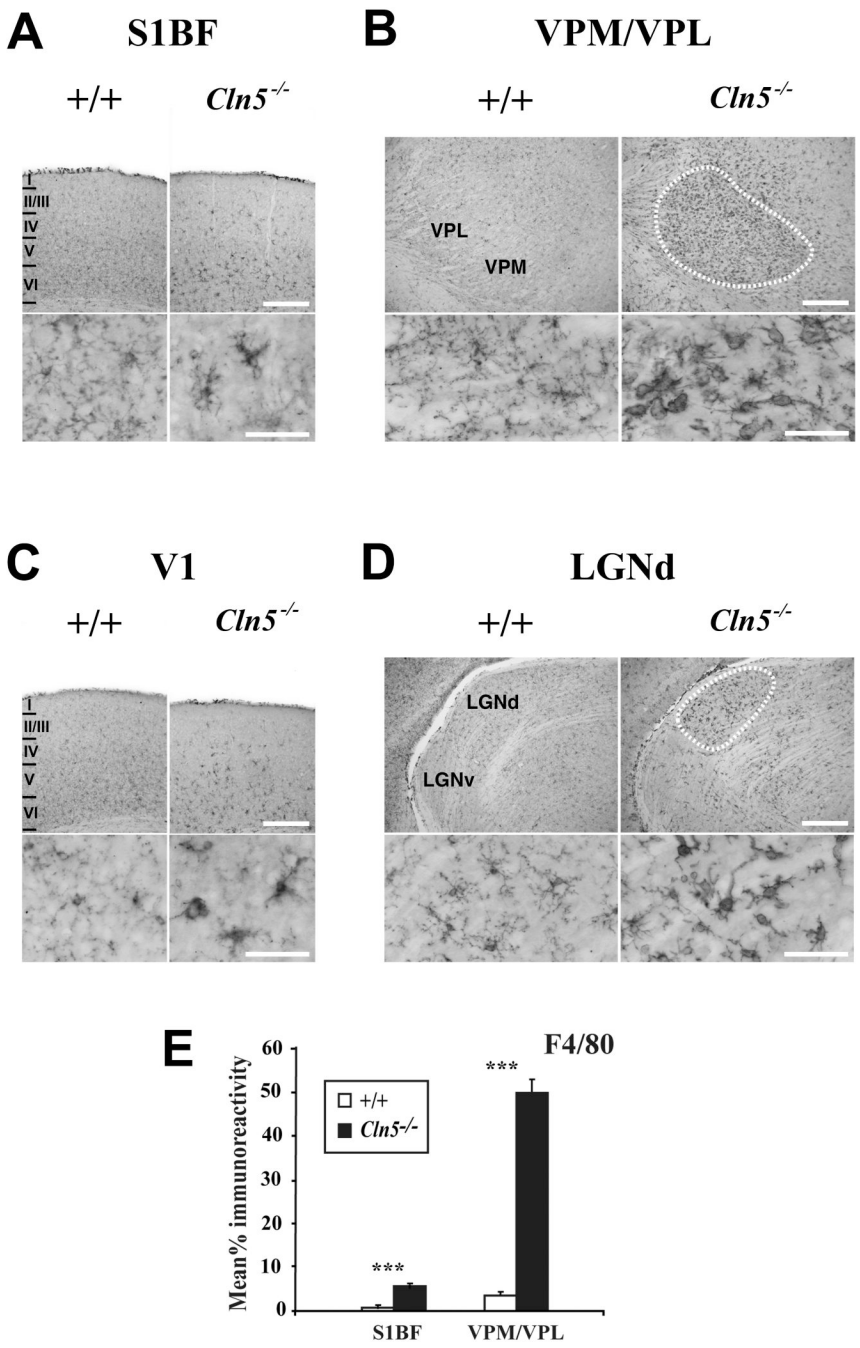

Figure 6.

Activation of microglia in 12 month old *Cln5* deficient mice. **(A, C)** Immunohistochemical staining for the microglial marker F4/80 reveals activated microglia to be more frequent within the deeper laminae (IV-VI) of the somatosensory cortex (S1BF, A) and primary visual cortex (V1, B) of *Cln5*$^{-/-}$ mice at 12 months of age compared to age matched control mice (+/+). In mutant mice, microglia displayed more intense F4/80 immunoreactivity with enlarged soma and fewer ramified processes (inserts), although complete transformation to brain macrophage like morphology was rare. Laminar boundaries are indicated by roman numerals. **(B, D)** Localized microglial activation within individual thalamic nuclei of 12 month old *Cln5*$^{-/-}$ mice is also revealed by F4/80 immunoreactivity. In these mutant mice, intensely stained F4/80

positive microglia with brain macrophage like morphology were present in the ventral posterior (VPM/VPL), nucleus (B) and dorsal lateral geniculate nucleus (D), but were virtually absent from adjacent thalamic nuclei (including the ventral lateral geniculate nucleus, LGNv) and were not present in age matched controls. The boundaries of these nuclei are indicated by white dashed lines. Scale bar = 300 μm; 50 μm in inserts. **(E)** Thresholding image analysis confirms the progressive and significant increase in F4/80 staining in both S1BF and VPM/VPL of *Cln5* deficient mice (*Cln5*$^{-/-}$) with increased age, compared to age matched controls (+/+). (mean±SEM; *** $p<0.001$; ANOVA with post-hoc Bonferroni analysis).

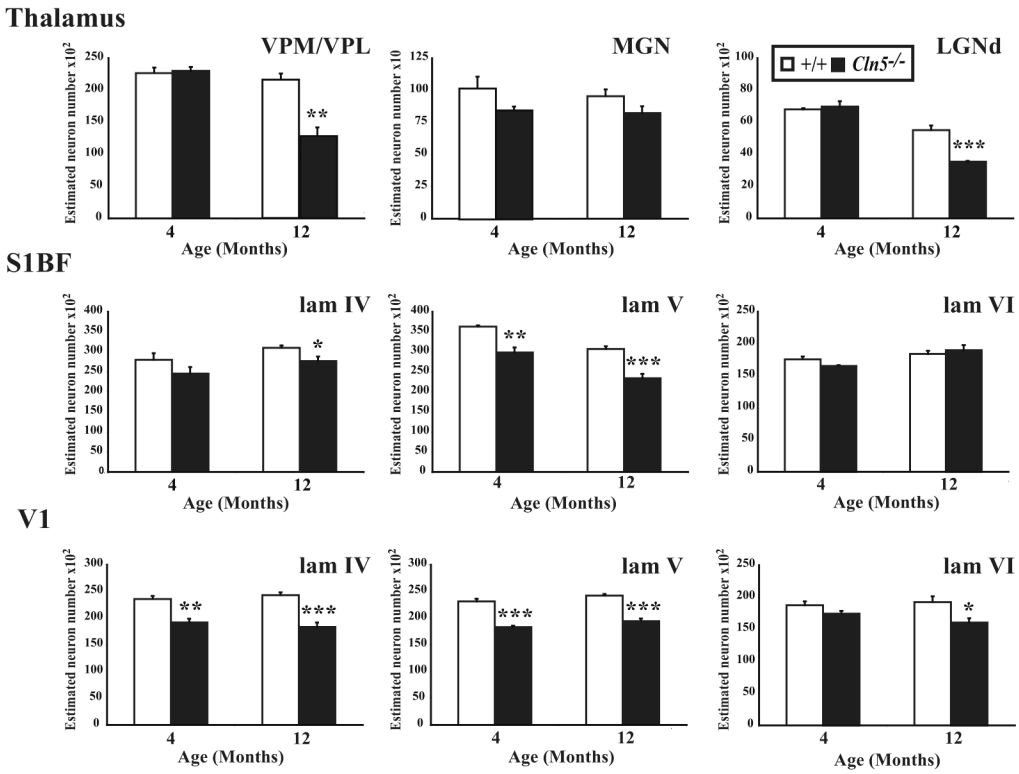

Figure 7.

Progressive loss of thalamic and cortical neurons in *Cln5* deficient mice. **(A)** Histograms of unbiased optical fractionator estimates of the number of Nissl stained thalamic relay neurons in the ventral posterior (VPM/VPL), medial geniculate nucleus (MGN), and dorsal lateral geniculate nucleus (LGNd), of *Cln5*$^{-/-}$ mice and age-matched controls (+/+) at different stages of disease progression. The number of neurons in VPM/VPL and LGNd nuclei declined in *Cln5*$^{-/-}$ mice with increased age, with significant neuron loss evident in these nuclei in 12 month old mutant mice. In contrast no significant loss of MGN neurons was observed in *Cln5*$^{-/-}$ mice at either age. (B, C) Histograms of unbiased optical fractionator estimates of the number of Nissl stained lamina IV granule neurons, lamina V pyramidal neurons and lamina VI feedback neurons in the somatosensory cortex (S1BF, B) and primary visual cortex (V1, C) of *Cln5*$^{-/-}$ mice and age-matched controls (+/+) at different stages of disease progression. Both cortical regions displayed a progressive loss of cortical neurons in mutant mice, but this occurred earlier and in all laminae of V1. A significant loss of laminae IV and V neurons was already apparent in V1 of *Cln5* deficient mice at 4 months of age, with additional significant neuron loss in lamina VI at 12 months of age. Neuron loss in S1BF progressed more slowly, but a significant loss of lamina V neurons was already evident in Cln5 deficient mice at 4 months of age, with an additional significant neuron loss in lamina IV of these mice at 12 months of age. (* $p<0.05$; ** $p<0.01$; *** $p<0.001$, ANOVA with post-hoc Bonferroni analysis).

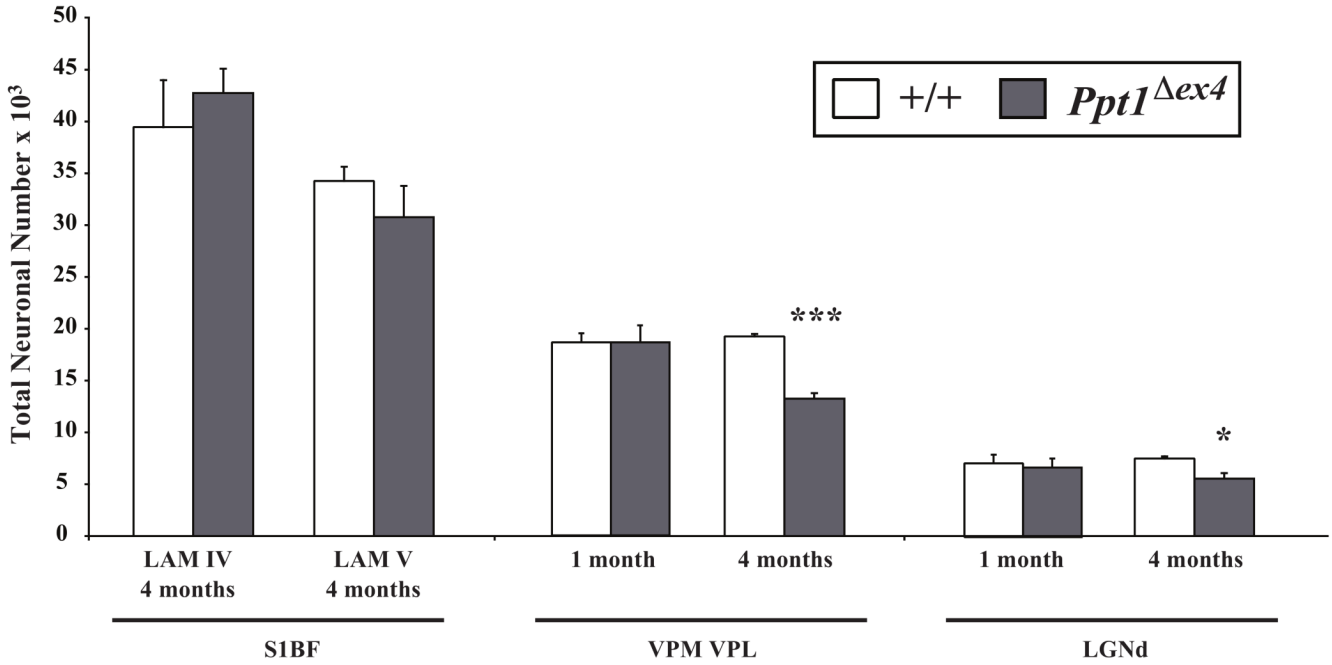

Figure 8.

Early loss of thalamic relay neurons in *Ppt1*$^{\Delta ex4}$ knock-in mice. Histograms of unbiased optical fractionator estimates of the number of Nissl stained lamina IV granule neurons and lamina V projection neurons in somatosensory barrelfield (S1BF) cortex; the ventral posterior nucleus of the thalamus (VPM/VPL), which provides afferent input to S1BF; and visual relay neurons in the dorsal lateral geniculate thalamic nucleus (LGNd) of *Ppt1*$^{\Delta ex4}$ mice and age-matched controls (+/+) at different stages of disease progression. No significant loss of cortical neurons in laminae IV or V of S1BF was evident in *Ppt1*$^{\Delta ex4}$ mice at either 1 or 4 months of age. In marked contrast, and consistent with the phenotype of *Ppt1*$^{-/-}$ mice (Kielar et al., 2007), a significant loss of both VPM/VPL and LGNd neurons was already observed at 4 months of age. (* $p<0.05$; *** $p<0.001$, ANOVA with post-hoc Bonferroni analysis).

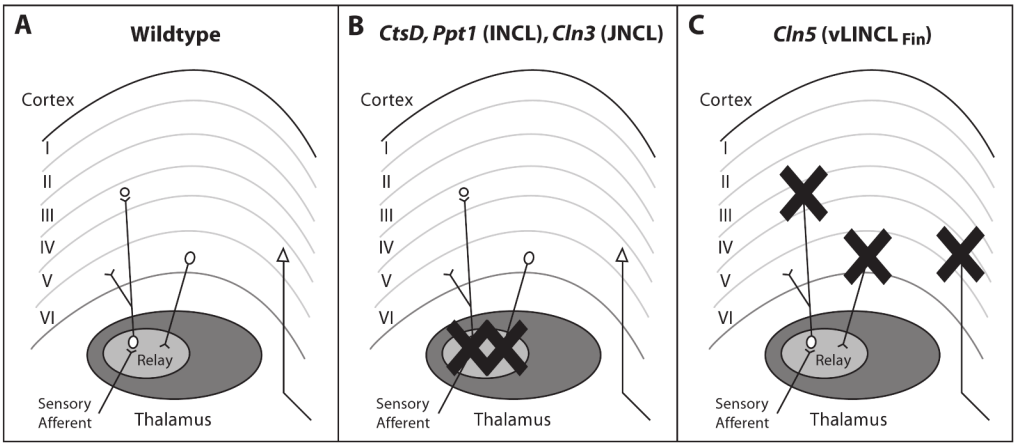

Figure 9.

Contrasting patterns of corticothalamic neuron loss in NCL mouse models. **(A)** Normal organization of thalamocortical pathways. Ascending sensory afferents terminate upon thalamic relay neurons, with one relay nucleus for information of different modalities. These relay neurons project mainly to lamina IV granule neurons of the appropriate cortical region, with collateral innervation of lamina VI. In turn, the cortex provides feedback projections to the thalamus from lamina VI, and lamina V neurons project outside this cortical region. **(B, C)** The thalamocortical system of all NCL mouse models displays progressive neuron loss. However, the timing and sequence in which these pathways are affected differs radically between forms of NCL. **(B)** In *Cathepsin D*, *Ppt1* and *Cln3* deficient mouse models the neuron loss begins in the thalamus and only subsequently occurs in the corresponding cortical region. **(C)** In contrast, neuron loss progresses in a completely opposite sequence in *Cln5* deficient mice. As this study reveals, neuron loss is first evident in the cortex of *Cln5*$^{-/-}$ mice, with loss of thalamic relay neurons occurring later in disease progression. However, regardless of the pattern of cell loss, visual pathways are consistently affected first in all NCL mouse models.